Nanoscale

RSC Publishing

PAPER

View Article Online
View Journal | View Issue

Cite this: *Nanoscale*, 2013, **5**, 5375

Tuning structural motifs and alloying of bulk immiscible Mo–Cu bimetallic nanoparticles by gas-phase synthesis†

Gopi Krishnan,*[a] Marcel A. Verheijen,[b] Gert H. ten Brink,[a] George Palasantzas[a] and Bart J. Kooi[a]

Received 31st January 2013
Accepted 4th April 2013

DOI: 10.1039/c3nr00565h

www.rsc.org/nanoscale

Nowadays bimetallic nanoparticles (NPs) have emerged as key materials for important modern applications in nanoplasmonics, catalysis, biodiagnostics, and nanomagnetics. Consequently the control of bimetallic structural motifs with specific shapes provides increasing functionality and selectivity for related applications. However, producing bimetallic NPs with well controlled structural motifs still remains a formidable challenge. Hence, we present here a general methodology for gas phase synthesis of bimetallic NPs with distinctively different structural motifs ranging at a single particle level from a fully mixed alloy to core–shell, to onion (multi-shell), and finally to a Janus/dumbbell, *with the same overall particle composition*. These concepts are illustrated for Mo–Cu NPs, where the precise control of the bimetallic NPs with various degrees of chemical ordering, including different shapes from spherical to cube, is achieved by tailoring the energy and thermal environment that the NPs experience during their production. The initial state of NP growth, either in the liquid or in the solid state phase, has important implications for the different structural motifs and shapes of synthesized NPs. Finally we demonstrate that we are able to tune the alloying regime, for the otherwise bulk immiscible Mo–Cu, by achieving an increase of the critical size, below which alloying occurs, closely up to an order of magnitude. It is discovered that the critical size of the NP alloy is not only affected by controlled tuning of the alloying temperature but also by the particle shape.

Introduction

Today's advances in technology rely increasingly on multi-functional nanostructured materials. Within this class of materials bimetallic structured nanoparticles (NPs) have attracted strong interest, because their functionality can be tuned using the detailed interplay of the two elemental components, which can provide a variety of particle shapes, morphologies, and compositions. Hence enhanced performance can be facilitated for diverse applications in many fields such as catalysis, optics, biodiagonistics and magnetic systems.[1–20] In this respect nano-alloying of two elements, which are largely immiscible in bulk, has attracted strong attention due to the fact that new functional properties can be tailored that are quite unique and distinct from those of the corresponding bulk metals and alloys.

Alloying of bulk immiscible elements is feasible in the nanoscale regime, because the enthalpy of mixing decreases with decreasing NP size and generally becomes negative below a certain size.[22–25] Besides the size effect, recent studies also suggest that the shape and the surface structure of NPs influence the alloying ability of immiscible materials.[21–24] Taking all these complex factors into consideration, the alloying ability of bulk immiscible compounds starts for NPs, depending on the composition selected, with size below 10 nm, while complete alloying (in the whole composition range) has been only observed for NPs with less than 2 nm size.[24] Phase segregation/core–shell formation is one of the major problems affecting the stability of the alloyed NPs when the NP size is increased above 2 nm. Consequently, alloying of bulk immiscible NPs with sizes beyond 10 nm is a formidable challenge and so far has not been reported. Here, however, we report that alloying of Mo–Cu NPs, which are bulk immiscible, is possible up to sizes of 60 nm by tuning the thermal environment and the cooling rate during NP growth.

Bimetallic NPs can have various structural motifs: (a) nano-alloy: random or ordered alloys in a mixed state and (b) core–shell, onion structure (multishell), Janus structure (dumbbell) in a segregated or phase-separated state.[25–30] These bimetallic structural motifs can be synthesized by various techniques including electrochemistry, chemical reduction and gas phase

[a]*Zernike Institute for Advanced Materials and the Materials Innovation Institute, University of Groningen, Nijenborgh 4, 9747 AG Groningen, The Netherlands. E-mail: gopi.k.krish@gmail.com*

[b]*Department of Applied Physics, Eindhoven University of Technology, P. O. Box 513, 5600 MB Eindhoven, The Netherlands*

† Electronic supplementary information (ESI) available: Experimental details including schematics of the gas phase synthesis set up, target arrangement, synthesis condition for various structures, and TEM images of alloy, core–shell and Mo–Cu–Mo onion nanoparticles. See DOI: 10.1039/c3nr00565h

synthesis.[25–33] Although gas phase synthesis of bimetallic NPs has recently received increased attention, because phase-separated NPs with clean high quality interfaces and surfaces can be produced,[31–33] the control of the various structures and shapes is still poorly understood. Nevertheless, the formation of various structural motifs for the same type of bimetallic NPs with *fixed chemical composition* (*e.g.* Mo–Cu) has not been reported so far because it is an extremely challenging task.

To address these challenges, we focus here on the Mo–Cu (bulk immiscible) NPs, because pure Mo NPs exhibit interesting self-organization phenomena to a decreasing surface energy of the system.[34–36] Indeed, Mo has a strong tendency to self-assemble into larger cubic particles from smaller structural sub-units of rhombic dodecahedrons or cubes.[34–36] It also has a size dependent crystal structure transformation from body centered cubic (bcc) to face centered cubic (fcc) as the NP size decreases.[36] Hence, using gas phase synthesis, with addition of Cu we report on the synthesis of Mo–Cu NPs with distinctively different structural motifs: core–shell, onion (multishell NPs), and alloy NPs at the single particle level with the same composition. Not only we tune the various structural motifs but we can also produce them with well-defined shapes like cube or spherical. Simultaneously we illustrate the possibility to extend the alloying NP size from 6 up to 60 nm, closely up to an order of magnitude, by proper tuning of the thermal environment and the cooling rate of the NPs during their growth.

Experimental methods

The Mo–Cu nanoparticles with various structural motifs and shapes were produced by the nanoparticle system nanosys500 from Mantis Deposition Ltd. (http://www.mantisdeposition.com). The sample chamber was evacuated to a base pressure of $\sim 1 \times 10^{-8}$ mbar with a partial oxygen pressure of $\sim 10^{-9}$ mbar. Super-saturated metal vapor is produced by magnetron sputtering of a sectioned target (Fig. 1 in the ESI†) consisting of ½ Mo and ½ Cu (99.95% purity of the Mo and Cu is obtained from Alpha Aesar) in an inert argon atmosphere (pressure of ~0.25 to 1.5 mbar depending on the choice of the structural motifs that were synthesized). The supersaturated metal vapor is then cooled by the Ar gas to form a nuclei which grow as nanoparticles. The nanoparticles formed in the aggregation volume are removed fast by the use of argon (Ar) which acts as a drift and sputter gas. The tuning of the thermal environment and energy was made by varying the discharge current and the pressure inside the aggregation volume (see Table 1 in the ESI†). The nanoparticles transported from the aggregation volume were deposited onto 25 nm thick silicon-nitride membranes, which were used for Transmission Electron Microscopy (TEM) analysis in a JEOL 2010F TEM.

Results and discussion

Fig. 1 shows transmission electron microscopy (TEM) and Scanning TEM (STEM) results for Mo–Cu alloy NPs directly synthesized in the gas phase by high pressure magnetron sputtering, while maintaining a specific discharge current (0.250 A; see ESI†). The principal difference in the synthesis conditions between Fig. 1(a–c) and (d–f) was the Ar gas flow rate of 40 and 70 sccm, and thus the pressure in the aggregation volume of the NP deposition source. This difference resulted in either cubic or spherically shaped NPs as shown by the bright field TEM images in Fig. 1(a) and (d), respectively. The presence of Mo–Cu bcc based solid solutions (alloy) for both particle shapes is confirmed by Fourier transform analysis of HRTEM images and electron diffraction patterns shown in Fig. 1(b) and (e) and Fig. 1(c) and (f).

Moreover, the measured interplanar distance in two orthogonal directions (110) and $(1\bar{1}0)$ in Fig. 1(b) is $d_{110} = 0.213 \pm 0.04$ nm. The latter deviates significantly from the one of pure Mo, which is $d_{110} = 0.222$ nm in both directions, and it agrees with a lattice spacing corresponding to a bcc based solid solution of Mo–Cu. Fig. 1(e) and (f) also show that the NPs contain a bcc solid solution of Mo–Cu. Compositional analysis by electron dispersive spectroscopy (EDS) in the TEM shows that the NPs consist of 86 ± 1 at.% of Mo and 14 ± 1 at.% of Cu. The EDS compositional analysis of randomly picked NPs with both cube and spherical shapes shows in all cases very similar compositions. Hence the difference in shape is not directly a compositional effect. The energy dispersive X-ray spectroscopy (EDX) mapping (in STEM mode) of the cube Mo–Cu alloy NPs, Fig. 1(g), also indicates that Cu and Mo are mixed within the NPs.

The Mo–Cu system is immiscible in its bulk form, and it has a positive enthalpy of formation of $\Delta H \sim 28$ kJ mol^{-1}. It is well known that immiscible metals in bulk can be alloyed in the nano-size regime, because the enthalpy of formation ΔH decreases with decreasing particle size, and it can become negative below a critical particle size ($\Delta H < 0$).[21–24] However, the critical size below which NPs start to form an alloyed structure depends on composition, shape, and surface effects thus yielding a critical size ≤10 nm.[21–24] Nonetheless in our case we observed alloying in Mo–Cu NPs with sizes ranging from 5 up to 60 nm for both the cube and spherical particle shapes. In view of the previous studies, it is not so surprising that we could produce alloyed Mo–Cu NPs with sizes of 6 ± 2 nm (Fig. 3(a) in the ESI†). However, the cube and spherical Mo–Cu NPs shown in Fig. 1 (which were produced without employing any particle mass filter) have an average diameter of ~59 ± 4 nm and ~32 ± 4 nm, respectively. Note the relatively monodisperse size distribution of NPs (~10% deviation) in the samples shown in Fig. 1.

In contrast to the earlier studies,[21–24] our results show that Mo and Cu are mixed in NPs having a size larger than 10 nm. Of course this can be attributed to our synthesis method (high pressure DC magnetron sputtering) which produces material out of thermodynamic equilibrium. Indeed, in the plasma temperatures beyond 3000 K can be reached, while very high cooling rates of the material are also present. One could expect that alloy NPs are formed in bulk immiscible systems, when mixing is still possible in the bulk liquid state. However, this mechanism cannot hold for bulk Mo–Cu, because even in the liquid state Mo–Cu is not miscible (only limited solubility of Cu in liquid Mo is possible). Nonetheless meta-stable alloy NPs can apparently be formed because of the strongly reduced

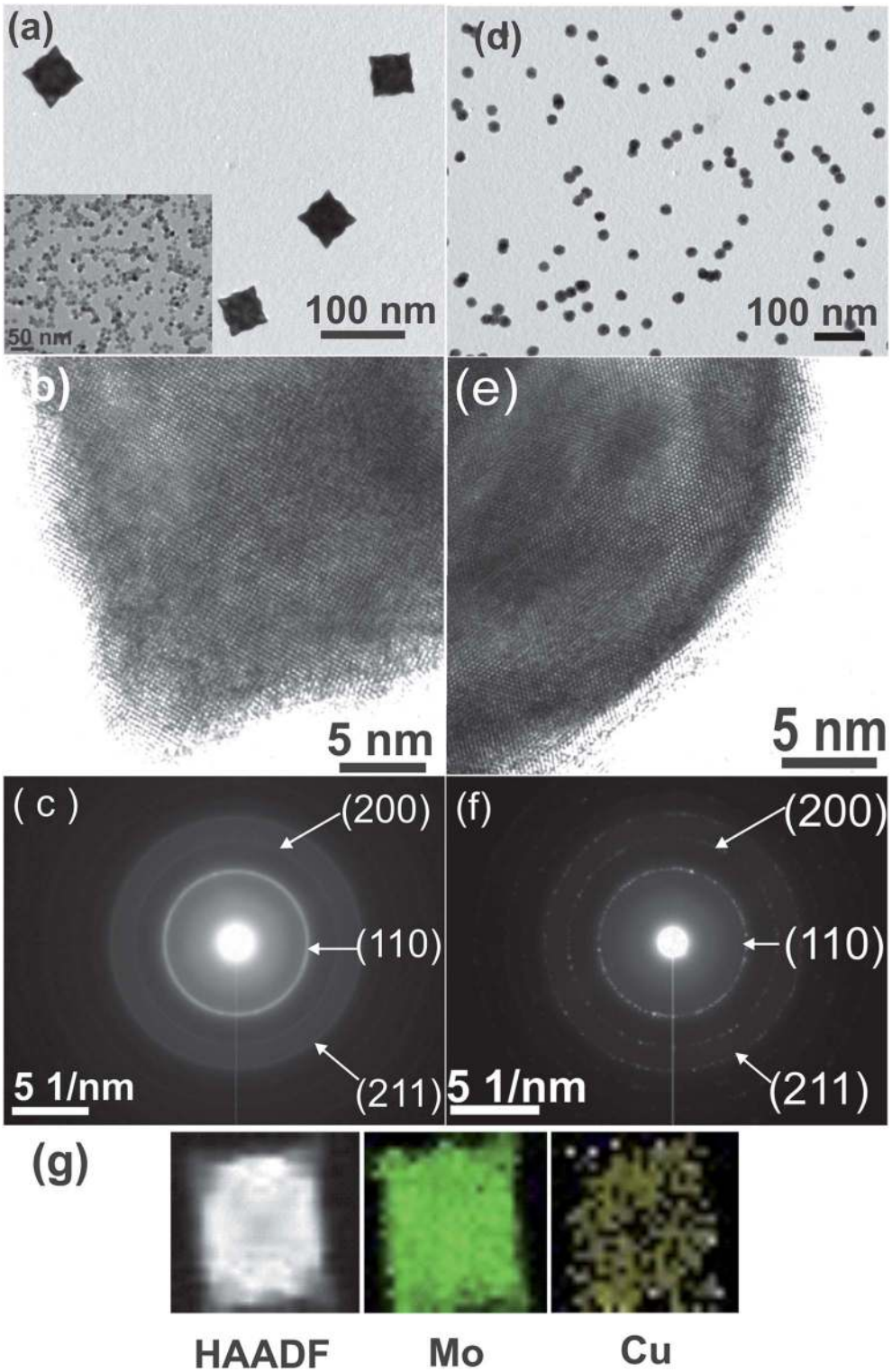

Fig. 1 Mo–Cu alloyed NPs synthesized in cube and spherical shapes with an average size of 59 ± 2 nm and 32 ± 3 nm, respectively. (a) Bright-field TEM image of the Mo–Cu alloyed NPs with a cube shape. The inset shows the low magnification TEM image of the same. (b) Corresponding HRTEM image of the Mo–Cu NPs. (c) Electron diffraction pattern of the cube Mo–Cu NPs with an alloyed structure. (d) Bright-field image of the Mo–Cu alloyed NPs with a spherical shape. (e) Corresponding HRTEM image of the alloyed NPs with a spherical shape. (f) Diffraction pattern of the alloyed NPs with a spherical shape showing the presence of the Mo–Cu alloyed structure. (g) Compositional (EDX) mapping of Mo and Cu for a cube shaped NP.

dimensions with a large surface to volume ratio. The surface-area difference model by Xiong *et al.*[24] shows that an increase of the critical size takes place with increasing temperature, while the enthalpy of formation can become negative, for NPs larger than 10 nm in size, which is in agreement with our current result.

In addition, our results also indicate that the shape of the NPs (with the same composition) affects the critical size for alloying of immiscible systems: a cube shape has a larger critical size than the spherical shape, *e.g.* Fig. 1. This is very similar to the work by Xiong *et al.*,[24] where they explained that on the basis of the shape factor. In order to understand the effect of composition on the critical size for alloying Mo–Cu, we have also varied the composition of the Mo–Cu sputtering targets to increase the Cu at.%. We found that NPs with an average composition of 76 ± 1 at.% Mo, 24 ± 1 at.% Cu and 70 ± 1 at.% Mo, 30 ± 1 at.% Cu (as determined by EDX) could only be alloyed with a critical size up to 20 and 16 nm, respectively (Fig. 3b and c in the ESI†). This means that the critical size for alloying decreases when the concentration of Cu is increasing from 14 to 30 at.% in Mo–Cu alloy nanoparticles and it could possibly increase further as the composition of Cu and Mo becomes more equivalent.[24]

Fig. 2(a) shows a bright field TEM image of the Mo–Cu core–shell NPs with both spherical and cube shapes produced together within the same deposition. Compared to the process used in the case of Fig. 1, the discharge current in the case of Fig. 2 was increased to 0.350 A (still using the same gas flow rate of 40 sccm). In this case it was possible to make core–shell NPs with a size distribution of ~19 ± 6 nm. However, core–shell NPs could also be produced with larger sizes than those shown for the alloy NPs in Fig. 1 (Fig. 4 in the ESI†). Fig. 2(b) shows the HRTEM image of the atomically resolved lattice spacing of d_{110} Mo core and the Cu-shell. Since Mo has a higher surface energy than Cu it is understood that particles with a Mo core and a Cu shell are produced. Comparing the Mo–Cu alloy and the Mo–Cu core–shell NPs we can infer that the energy supplied or energy gained by the NPs during their growth, and the thermal environment they experience, has significant influence on their structure.

Understanding how this behavior is related to the process conditions can provide the "*know-how*" to tune different structures for a chosen bimetallic system. Therefore, we will try to obtain more insight into the NP formation process. Indeed, the process starts with the vaporization of the bi-metallic target with a bombardment of Ar ions. In the next step the evaporated energetic atoms collide with Ar molecules and/or drift gas (*e.g.* He) to lose their energy (thermalize) and form NP nuclei. Formation of the latter starts immediately after collision of the high energetic metal atoms with low energy Ar gas atoms, because there is a large drop in temperature and energy during collisions. Then the nuclei grow by a collision/aggregation process to form NPs. Normally at a high cooling rate (high Ar gas flow rate) the NPs are quenched very fast and remain in their high temperature state, which means that there is not sufficient time/energy for atomic diffusion to occur. Hence if we can cool the NPs slowly, sufficient atomic diffusion within the particles can occur resulting in large variations of the final NP structure. Fig. 3(a) shows schematically relevant details of the bimetallic NP formation based on our gas phase synthesis process and the

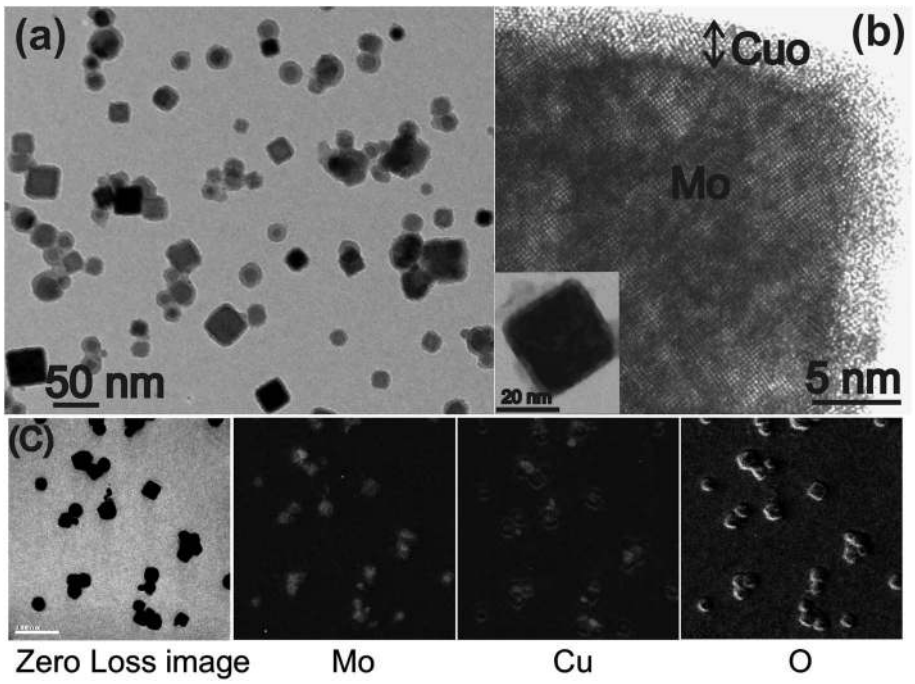

Fig. 2 (a) Bright-field TEM image of the Mo–Cu core–shell NPs with both spherical and cube shapes, $I = 0.35$ A and Ar flow = 40 sccm. (b) HRTEM image of the Mo–Cu core–shell NPs showing d_{110} resolved lattice spacing in the Mo core and the Cu shell. The inset shows the bright field TEM image of the same NP. (c) Energy filtered (GIF) TEM imaging showing Mo, Cu and O elemental maps (based on the three window technique) for the Mo–Cu core–shell NPs.

various chemical orderings that can be achieved within the NPs. Fig. 3(b) shows schematically the temperature drop/cooling rate of NPs with respect to the time of flight and for different Ar gas flow rates. The sharp drop in the temperature after a certain time indicates that NPs are at the edge of the plasma region where the temperature drops very rapidly. Thus the thermal energy involved during the formation and growth of NP nuclei can be tuned opening the possibility to produce different structured NPs with the same composition.

During sputtering the energy that we can supply to the sputtered metal atoms through the Ar ions can be varied by using different discharge voltages and/or currents. Increasing the discharge current will increase the plasma density, which not only increases the energy of the growing species but also influences the temperature in the plasma and the cooling rate of NPs. This is because the energy dissipation rate between metal atoms and the more energetic Ar molecules (due to bombardment of highly energetic Ar ions) is reduced. Thus varying the discharge current and Ar gas flow (pressure) we can tune the temperature and the cooling rate along with the energy of the growing species. Indeed, Fig. 3(c) shows a plausible overview of the different structural motifs of Mo–Cu that we could synthesize in a controlled and reproducible manner. Fig. 3(d) gives an illustration of how the influence of thermal energy (different discharge current) can be utilized to prepare different motifs for a constant low gas flow rate.

Having this background information, we will attempt to understand the reason behind the formation of Mo–Cu alloy and Mo–Cu core–shell structures, *e.g.* in Fig. 1 and 2. Initially, for the two flow rates (40 and 70 sccm) in Fig. 1 cube and spherical shaped alloy particles are formed. However, with low gas flow rates reconstruction to cube shaped particles can occur during cooling, which is the expected morphology for pure Mo particles.[34–36] With higher gas flow rates there is insufficient time for the reconstruction and the particles remain spherical as observed. Although at the relatively low discharge current (~0.250 A) the energy gained by Cu atoms in the plasma is just sufficient for mixing and formation of Mo–Cu solid solution, it is not sufficient to overcome the energy barrier leading to phase separation and Mo–Cu core–shell formation. The same result was also observed in the case of MoCu thin films, where only after annealing above 500 °C phase separation and precipitation

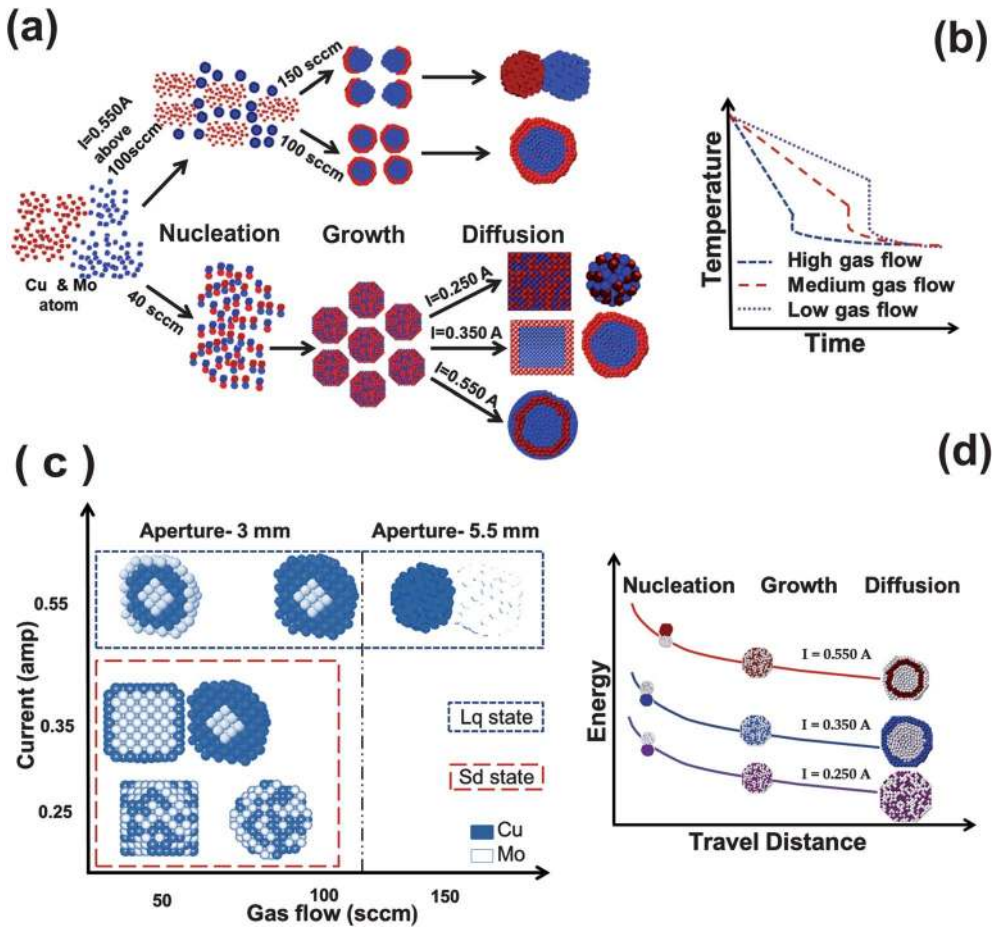

Fig. 3 Schematic representation of the Mo–Cu NP formation including tuning of various structural motifs by controlling the thermal environment experienced by the NPs. (a) Formation mechanism of Mo–Cu NPs with various types of chemical ordering. (b) Effect of the gas flow rate (pressure) on the cooling rate experienced by the NPs. (c) The table shows the various structural motifs and shapes of Mo–Cu synthesized at various discharge currents and gas flow rates, Lq – Liquid state and Sd – Solid state indicate the NP formation state, the aperture size used for producing various structures is indicated as 3.0 and 5.5 mm. (d) Effect of the energy supplied (*via* discharge current) on various synthesized structures at a constant flow rate of Ar (*e.g.*, 40 sccm in the present case).

of Cu were observed.[37] Similarly, when we increase the discharge current or energy of the growing metal atoms it might be possible to form a core–shell structure for the same other settings. In fact this was achieved in the case of Fig. 2 by increasing the discharge current to 0.350 A. As a result the Cu atoms had sufficient energy to segregate to the surface and to enable phase separation. Previous studies have shown oxidation driven de-alloying in Ag–Au alloy samples kept out of vacuum over an extensive period of time up to 2 years.[38] However, in our case the TEM analysis of the freshly prepared samples was completed in less than a week. Moreover, we examined the same Mo–Cu alloy NPs after six months and their structure remained unchanged, where the alloy was surrounded by an oxide shell. This confirms the fact that the Mo–Cu core–shell structure is formed during the production of NPs.

From the results depicted in Fig. 1 and 2 we can understand that by further increasing the discharge current to 0.550 A at 40 sccm, one would expect a Janus shaped (dumbbell) or a core–shell structure to form. Contrary to that Fig. 4 shows that these structures are not formed, but instead an onion structure Mo–Cu–Mo is formed. Fig. 4(a) shows the bright field TEM image of the relatively monodisperse Mo–Cu–Mo NPs. The HRTEM image in Fig. 4(b) and the fast Fourier transform (FFT) image in Fig. 4(c) confirm that the onion structure is formed and consists of pure Mo and Cu shells. The FFT pattern displays double spots in the radial direction of the particle. This can be indexed using a combination of a Mo⟨111⟩ zone axis pattern and Cu(111) spots. The alignment of the Mo(110) and Cu(111) spots implies an epitaxial relationship between two elements. The HRTEM image also provides evidence for a hetero-epitaxy, as the crystal planes cross the alternating bright and dark contrast zones assigned to the different elements. This epitaxial relationship was previously reported by Mundschau *et al.*[39] Both HRTEM images and diffraction patterns yielded lattice spacings that correspond to only pure Mo and Cu excluding Mo–Cu alloy formation. This holds for most of the NPs produced under these conditions (see Fig. 5(a) in the ESI†). The contrast in the HRTEM image also shows the presence of the two different shells containing only Cu and Mo. The contrast originates from compositional variation and it is not related to the thickness effects as observed previously by Ferrer *et al.* for multishell AuPd NPs.[39] We observed the onion structure only for bigger NPs, which is similar to the other reported studies since phase segregation occurs for bigger NPs.[33,40]

The principal reason for onion structure formation is likely related to the fact that with a higher discharge current the NPs nucleate and grow in the liquid state. By contrast in the previous cases (*e.g.*, Fig. 1 and 2) the NPs were formed in the solid state. Fig. 5 shows schematically the formation mechanism of the onion structures. The large size and spherical shape of the particles also reflect the liquid phase origin of the NPs. The excess kinetic energy has been used in the process of growth by collision of Mo and Cu nuclei and this in turn causes the melting of the NPs. During solidification, Mo will tend to solidify first, because it has a higher melting point than Cu (T_{Mo} = 2890.15 K/T_{Cu} = 1356.15 K). Solidification in a NP is a surface phenomenon (solidification occurs by collision with

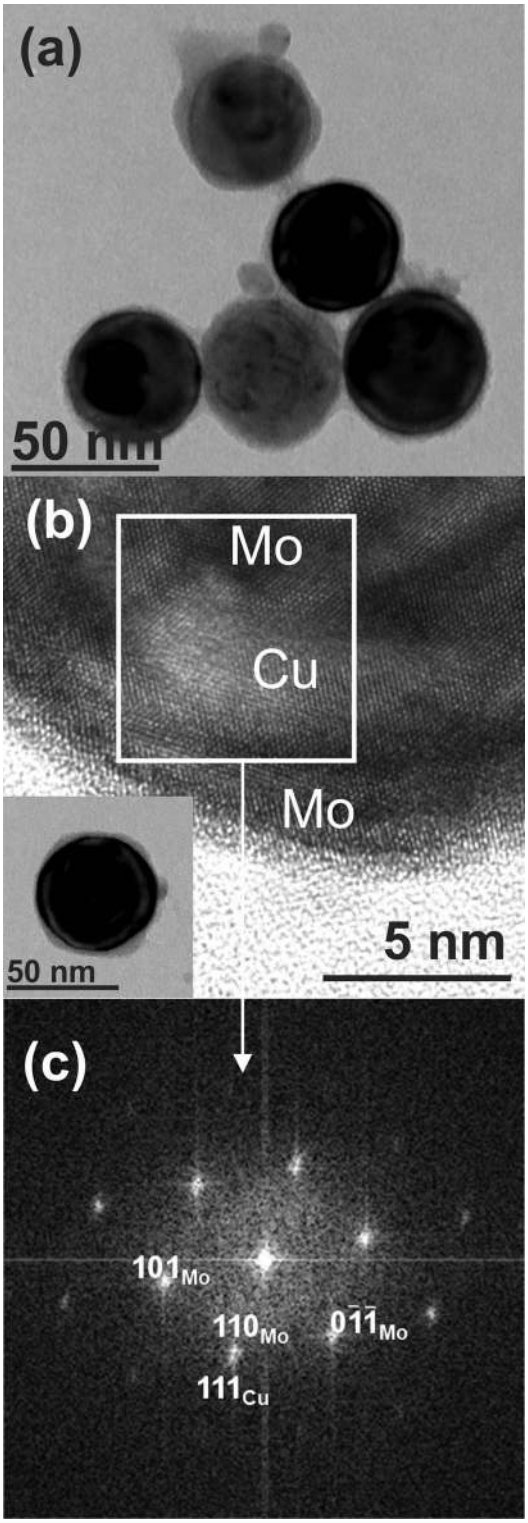

Fig. 4 (a) Bright field TEM image of the Mo–Cu–Mo onion structured (multishell) NPs, I = 0.55 A and Ar flow = 40 sccm. (b) HRTEM image of the Mo–Cu–Mo showing the presence of Mo and Cu. The inset shows the bright field TEM image of the corresponding NP. (c) Fourier transform image of part of the HRTEM image in (b) indexed using a combination of a Mo⟨111⟩ zone axis pattern and Cu(111) spots shows the presence of Mo(110) and Cu(111).

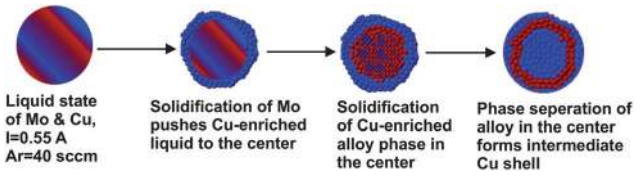

Fig. 5 Schematic illustration of the formation mechanism of Mo–Cu–Mo onion structures.

external species like Ar gas atoms) that leads to Mo solidification at the surface, while it drives Cu to the center of the NPs.[33] Also from the literature it has been identified that the preferred sites for Cu growth inside the NPs are at the subsurface (just below the surface of the NPs) or at the center of the NPs.[30,41] Therefore Cu does not have sufficient energy or time to reach the surface, since the diffusion of Cu atoms starts from the interior of the NPs (in the liquid state Cu is pushed to the center of the NPs during slow solidification), and as a result it only gives rise to an intermediate layer of Cu in agreement with our observations.

Fig. 6(a) shows Mo–Cu core–shell NPs with a spherical shape having a size (distribution) of $\sim 16 \pm 4$ nm. To form these core–shell NPs with only one kind of morphology say spherical, we have used the highest discharge current of 0.550 A so that the NPs can grow in the liquid state. Note the difference between Fig. 2 and 6, where in Fig. 2 both spherical and cube shaped NPs are present, whereas in Fig. 6 only the spherical morphology is present. Compared to Fig. 4, which corresponds to the same discharge current, here a much higher gas flow rate was used (100 sccm; 40 sccm in Fig. 4). Simultaneously as the cooling from high temperatures is rapid, the atoms lose their energy very rapidly during NP nucleation. Under these conditions only Mo is able to form stable nuclei. This is due to the fact that the kinetic energy of the sputtered Cu atoms is always higher than Mo due to its high energy transfer function and lower bond energy.[32,43,44] Simultaneously the high Ar gas flow rate (velocity of the NPs is proportional to the gas flow rate before the aperture of the aggregation volume is reached) will increase the velocity of the NPs forcing them to move faster out of the plasma region. As a result Cu does not have sufficient time to lose efficiently its kinetic energy and form stable nuclei. Instead, Cu grows on Mo that is serving as the nuclei for the Cu shell, similar to the observation by Yin *et al.*[32,41,42] This conclusion is also based on the experimental fact that we do not observe any Cu NPs under these conditions. Fig. 6(b) shows a HRTEM image of the Mo–Cu core–shell NPs (where the Cu-oxide shell is formed during *ex situ* transfer to the TEM). By increasing the Ar gas flow rate further to 150 sccm, we were able to achieve a very thin Cu-oxide shell as observed in TEM of only $\sim$1 to 2 nm thickness. The thinner Cu shell is the result of the high velocity of NPs leaving faster the plasma region. Therefore, this method (with variation of the gas flow rate) can be effectively employed to tune the Cu shell thickness around the Mo core.

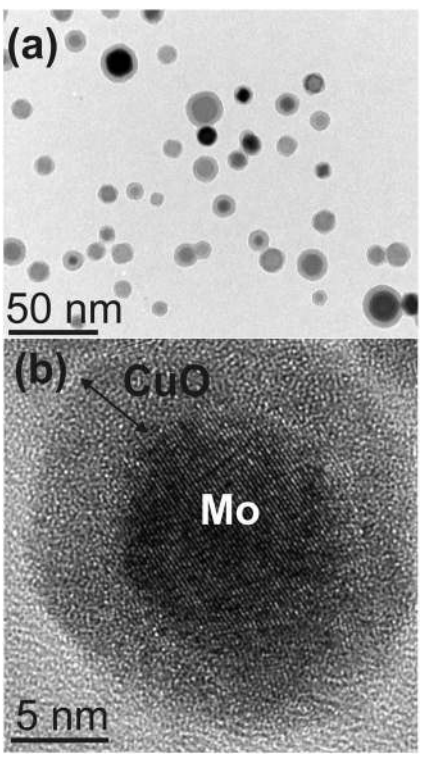

Fig. 6 Mo–Cu core–shell NPs with only spherical shape, $I = 0.55$ A and Ar flow = 100 sccm. (a) Bright field TEM image of the Mo–Cu NPs with an average size of 16 ± 4 nm. (b) HRTEM image of the Mo core with (110) atomic planes resolved and with an amorphous Cu-oxide shell (which is possibly formed during *ex situ* transfer to the TEM).

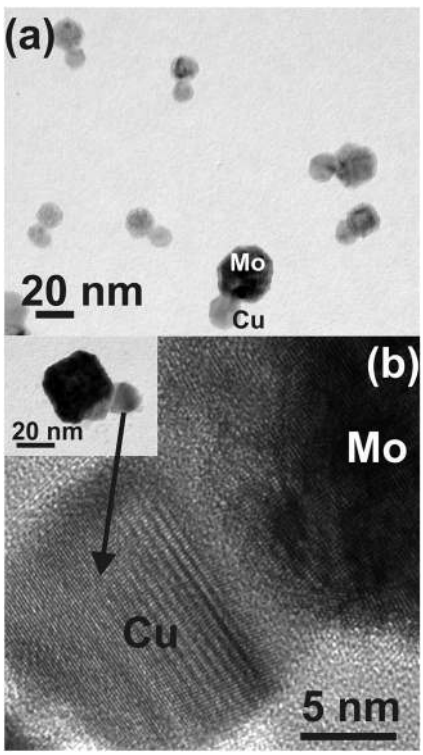

Fig. 7 (a) Bright field TEM image of Mo–Cu Janus type NPs, $I = 0.55$ A and Ar flow = 150 sccm (aperture size = 5.5 mm). (b) HRTEM image showing a phase separated Janus structure with the Cu(111) and Mo(110) lattice spacings resolved. The inset shows the corresponding NP at a lower magnification.

By maintaining the same discharge current, but increasing the flow rate of Ar (150 sccm) further and increasing the aperture size (5.5 mm) at the end of the aggregation volume (see ESI†), finally we were able to synthesize Mo–Cu NPs with a Janus/dumbbell structure. The principle for achieving this set of particles is the same as that described for the NPs shown in Fig. (6). The larger aperture (thus increasing the pumping rate of the aggregation volume through the aperture) increases the velocity of the emerging NP and in turn reduces the time for Cu to completely coat the Mo core. As a result a Janus type Mo–Cu structural motif emerges as is shown by the HRTEM image in Fig. 7.

Conclusions

We have presented a gas phase method for tuning the structural motifs of otherwise bulk immiscible Mo–Cu NPs having both high quality and clean surfaces/interfaces. This method is feasible by tailoring the plasma energy, the cooling rate, and the diffusion process experienced by the NPs during their gas synthesis. The structural motifs range from completely alloyed particles with either cube or spherical shape, Mo–Cu core–shell particles with cube or spherical shape, spherical 'onion' Mo–Cu–Mo particles (intermediate Cu shell), and Janus/dumbbell type Mo–Cu NPs. The critical size for alloying Mo–Cu, *e.g.* for forming NPs in which Mo and Cu are completely mixed, is in our work considerably larger (closely to an order of magnitude) than has been reported before for bulk immiscible binary NPs. In this case also an effect of shape was observed, because alloyed cube particles were observed to be larger (having thus a larger critical size) than alloyed spherical particles. In principle, the method proposed in the present work can be extended to other bimetallic systems in order to tune NPs with different types of chemical ordering important for a wide range of research fields and applications in nanoplasmonics, catalysis, biodiagnostics, and nanomagnetics.

Acknowledgements

We would like to acknowledge the support of this work by The Netherlands Institute of Fundamentals Research for Materials (FOM).

References

1 J. P. Wilcoxon and B. L. Abrams, *Chem. Soc. Rev.*, 2006, **35**, 1162.
2 R. Fernando, J. Jellinek and R. Johnston, *Chem. Rev.*, 2008, **108**, 845.
3 A. E. Russell and A. Rose, *Chem. Rev.*, 2004, **104**, 4613.
4 V. R. Stamenkovic, B. Fowler, B. S. Mun, G. F. Wang, P. N. Ross, C. A. Lucas and N. M. Markovic, *Science*, 2007, **315**, 493.
5 E. Prodan and P. Nordlander, *Nano Lett.*, 2003, **3**, 543.
6 V. Skumryev, S. Stoyanov, Y. Zhang, G. Hadjipanayis, D. Givord and J. Nogues, *Nature*, 2003, **423**, 850.
7 C. Burda, X.-B. Chen, R. Narayanan and M. A. El-Sayed, *Chem. Rev.*, 2005, **105**, 1025.
8 C. N. R. Rao, G. U. Kulkarni, P. J. Thomas and P. P. Edwards, *Chem. Soc. Rev.*, 2000, **29**, 27.
9 Z. Y. Li, J. P. Wilcoxon, F. Yin, Y. Chen, R. E. Palmer and R. L. Johnston, *Faraday Discuss.*, 2008, **138**, 363.
10 S. Alayoglu and B. Eichhorn, *J. Am. Chem. Soc.*, 2008, **130**, 17479.
11 F. Tao, M. E. Grass, Y. Zhang, D. R. Butcher, J. R. Renzas, Z. Liu, J. Y. Chung, B. S. Mun, M. Salmeron and G. A. Somorjai, *Science*, 2008, **322**, 932.
12 S. E. Habas, H. Lee, V. Radmilovic, G. A. Somorjai and P. Yang, *Nat. Mater.*, 2007, **6**, 692.
13 S. Piccinin, S. Zafeiratos, C. Stampfl, T. W. Hansen, M. Havecker, D. Teschner, V. I. Bukhtiyarov, F. Girgsdies, A. Knop-Gericke, R. Schl€ogl and M. Scheffler, *Phys. Rev. Lett.*, 2010, **104**, 035503.
14 D. Zitoun, M. Respaud, M. C. Fromen, M. J. Casanove, P. Lecante, C. Amiens and B. Chaudret, *Phys. Rev. Lett.*, 2002, **89**, 037203.
15 L. M. Liz-Marzan, *Langmuir*, 2006, **22**, 32.
16 D. Alloyeau, C. Ricolleau, C. Mottet, T. Oikawa, C. Langlois, Y. Le Bouar, N. Braidy and A. Loiseau, *Nat. Mater.*, 2009, **8**, 940.
17 W. H. Binder, *Angew. Chem., Int. Ed.*, 2005, **44**, 5172.
18 Z. M. Peng and H. Yang, *J. Am. Chem. Soc.*, 2009, **131**, 7542.
19 S. Kim, S. K. Kim and S. Park, *J. Am. Chem. Soc.*, 2009, **131**, 8380.
20 Y. Vasquez, A. K. Sra and R. E. Schaak, *J. Am. Chem. Soc.*, 2005, **127**, 12504.
21 L. H. Liang, G. W. Yang and B. W. Li, *J. Phys. Chem. B*, 2005, **109**, 16081.
22 S. Xiao, W. Hu, W. Luo, Y. Wu, X. Li and H. Deng, *Eur. Phys. J. B*, 2006, **54**, 479.
23 J. M. Martinez De La Hoz, R. C. Tovar and P. B. Balbuena, *Mol. Simul.*, 2009, **35**, 785.
24 S. Xiong, W. Qi, B. Huang and M. Wang, *ChemPhysChem*, 2011, **12**, 1317.
25 S. Darby, T. V. Mortimer-Jones, R. L. Johnston and C. Roberts, *J. Chem. Phys.*, 2002, **116**, 1536.
26 F. Chen, B. C. Curley, G. Rossi and R. L. Johnston, *J. Phys. Chem. C*, 2007, **111**, 9157.
27 M. Zhang and R. Fournier, *THEOCHEM*, 2006, **762**, 49.
28 M. D. L. Hoz, J. M. Tovar, R. Callejas and P. Balbuena, *Mol. Simul.*, 2009, **35**, 785.
29 G. Rossi, A. Rapallo, C. Mottet, A. Fortunelli, F. Baletto and R. Ferrando, *Phys. Rev. Lett.*, 2004, **93**, 105503.
30 F. Baletto, C. Mottet and R. Ferrando, *Phys. Rev. Lett.*, 2003, **90**, 135504.
31 J.-M. Qiu and J. P. Wang, *Adv. Mater.*, 2007, **19**, 1703.
32 F. Yin, Z. W. Wang and R. E. Palmer, *J. Am. Chem. Soc.*, 2011, **133**, 10325.
33 Y.-H. Xu and J.-P. Wang, *Adv. Mater.*, 2008, **20**, 994.
34 A. S. Edelstein, G. M. Chow, E. I. Altman, R. J. Colton and D. M. Hwang, *Science*, 1991, **251**, 1590.
35 F. H. Kaatz, G. M. Chow and A. S. Edelstein, *J. Mater. Res.*, 1993, **8**, 995.
36 T. Vystavel, S. A. Koch, G. Palasantzas and J. Th. M. De Hosson, *Appl. Phys. Lett.*, 2005, **86**, 113113.

37 G. Ramanath, H. Z. Xiao, L. C. Yang, A. Rockett and L. H. Allen, *J. Appl. Phys.*, 1995, **78**, 2435.
38 D. Belić, R. L. Chantry, Z. Y. Li and S. A. Brown, *Appl. Phys. Lett.*, 2011, **99**, 171914.
39 M. Mundschau, E. Bauer and W. Świech, *J. Appl. Phys.*, 1989, **65**, 581.
40 D. Ferrer, A. Torres-Castro, X. Gao, S. Sepúlveda-Guzmán, U. Ortiz-Méndez and M. José-Yacamán, *Nano Lett.*, 2007, **7**, 1705.
41 G. Krishnan, G. Palasantzas and B. J. Kooi, *Appl. Phys. Lett.*, 2010, **97**, 131911.
42 G. Krishnan, G. Palasantzas and B. J. Kooi, *Appl. Phys. Lett.*, 2010, **97**, 261912.
43 B. Chapman, *Glow Discharge Processes*, Wiley, New York, 1980.
44 T. J. Konno, S. Yamamuro and K. Sumiyama, *J. Vac. Sci. Technol., B*, 2002, **20**, 834.